



31 **Key points:**

- 32 • Ocean coupling generally leads to decreased tropical cyclone (TC) precipitation over both  
33 ocean and land
- 34 • Large-scale sea surface temperature biases and TC cold wakes, key facets of ocean  
35 coupling, drive the precipitation decline
- 36 • Projected future TC precipitation increases in most regions, however the magnitude can  
37 vary by a factor of 3 depending on ocean coupling

38

39 **Abstract:** This study aims to quantify the impacts of ocean coupling on simulated and projected  
40 tropical cyclone (TC) precipitation in the Northern Hemisphere. We used global climate model  
41 (GCM) simulations over 1950–2050 from the High Resolution Model Intercomparison Project  
42 (HighResMIP) and compared its fully coupled atmosphere–ocean GCMs (AOGCMs) with  
43 atmosphere-only GCMs (AGCMs). We find that ocean coupling generally leads to decreased TC  
44 precipitation over ocean and land. Large-scale sea surface temperature (SST) biases are critical  
45 drivers of the precipitation difference, with secondary contributions from local TC–ocean  
46 feedbacks via SST cold wakes. The two driving factors, attributed to ocean coupling in the  
47 AOGCMs, influence TC precipitation in association with decreased TC intensity and specific  
48 humidity. The AOGCMs and AGCMs consistently project TC precipitation increases in 2015–  
49 2050 relative to 1950–2014 over ocean for all basins, and for landfalling TCs in the North Atlantic  
50 and western North Pacific.

51

52 **1. Introduction**

53 Heavy precipitation and associated floods from tropical cyclones (TCs) have caused enormous  
54 damages to the economy and human health (Bell et al., 2018; Rappaport, 2014; Rappaport &  
55 Blanchard, 2016). Globally, TCs have resulted in US\$23 billion of economic damages (adjusted  
56 to current value) and more than 9,500 fatalities per year over the past half a century (CRED, 2021),  
57 with excessive precipitation as one of the leading causes (Bakkensen et al., 2018; Bell et al., 2018).  
58 Among the 2544 lives in the US claimed by Atlantic TCs over 1963–2012, about a quarter of the  
59 fatalities was attributed to TC precipitation (TCP)-induced floods and mudslides (Rappaport,  
60 2014). Moreover, extreme precipitation (>750 mm) from Hurricane Harvey in 2017 caused  
61 unprecedented flooding over the greater Houston area, making the hurricane one of the costliest

62 disasters (US\$131 billion) in US history (NOAA National Centers for Environmental Information,  
63 2021). Future climate change may double the economic damages of TCs by 2100 primarily through  
64 increased TC intensity, storm surge, and precipitation rate (Knutson et al., 2020; Mendelsohn et  
65 al., 2012; Patricola & Wehner, 2018). Therefore, it is imperative to accurately predict TCP and  
66 assess the risk with changing TCP.

67  
68 Global climate models (GCMs), especially high resolution models (50 km and higher), are  
69 important tools to simulate and project TCs (Haarsma et al., 2016; Li & Srivier, 2018; Walsh et al.,  
70 2016; Wehner et al., 2015). But there exist large uncertainties in simulated TCs and associated  
71 precipitation, which are rooted in model physics, resolution, and experimental design (Hasegawa  
72 & Emori, 2007; Li & Srivier, 2018, 2019; Roberts et al., 2020a; Roberts et al., 2020b; Zhang, W.,  
73 et al., 2021). In particular, atmosphere–ocean interactions in GCMs are a major source of  
74 uncertainty (Li & Srivier, 2018, 2019; Roberts et al., 2020b). Active atmosphere–ocean  
75 interactions, as observed in the real world and simulated by coupled atmosphere–ocean GCMs  
76 (AOGCMs), are crucial in correctly representing TC intensity, duration, and precipitation (Li &  
77 Srivier, 2018; Ma et al., 2020; Scoccimarro et al., 2017c; Vincent et al., 2012a; Zarzycki, 2016).  
78 Strong TC–ocean interactions usually cool sea surface temperatures (SSTs) along TC tracks due  
79 to strong winds of TCs (Vincent et al., 2012a). The winds vertically mix and entrain surface warm  
80 water with lower-level colder water and enhance upwelling and ocean–atmosphere heat fluxes  
81 (Liu et al., 2011; Price, 1981; Vincent et al., 2012a). The TC-induced SST cooling (cold wakes) is  
82 approximately 1°C on average and affects at least five radii of maximum wind (Vincent et al.,  
83 2012a). As TCs obtain energy from the upper ocean, cold wakes generate a negative feedback to  
84 TCs via modulating enthalpy flux and regional atmospheric circulation (Karnauskas et al., 2021;  
85 Kushnir et al., 2002; Ma et al., 2020; Trenberth et al., 1998; Vincent et al., 2012b; Zarzycki, 2016).  
86 Therefore, they impose profound effects on TC characteristics and TCP (Karnauskas et al., 2021;  
87 Li & Srivier, 2019; Ma et al., 2020; Zarzycki, 2016). Cold wakes were found to decrease post-TC  
88 precipitation by 17% in the wakes (Ma et al., 2020). They can reduce the frequency of subsequent  
89 TCs by 10% and shorten the return period of Category 5 hurricanes by a factor of six across the  
90 North Atlantic (Karnauskas et al. 2021).

91

92 While AOGCMs are capable of simulating TC–ocean interactions, they produce large-scale SST  
93 biases (Richter, 2015; Richter & Tokinaga, 2020; Zhu et al., 2020) which can cause a substantial  
94 misrepresentation of TC activity (Hsu et al., 2019; Zhang, G., et al., 2021). This deficiency leads  
95 to the common use of prescribed-SSTs with atmosphere-only GCMs (AGCMs), which by  
96 definition lack ocean coupling and therefore simulated cold wakes (Haarsma et al., 2016; Hsu et  
97 al., 2019; Roberts et al., 2020a; Vincent et al., 2012a). The difference in ocean coupling between  
98 AGCMs and AOGCMs generates disparate TC activity and TCP (Hasegawa & Emori, 2007; Li &  
99 Sriver, 2018, 2019; Roberts et al., 2020b; Zarzycki, 2016). For example, Roberts et al. (2020b)  
100 found that for the North Atlantic TCs during 1979–2014, most AOGCMs underestimated its  
101 frequency by 16.7–80% as compared to AGCMs. While AGCMs predicted future increases in TC  
102 frequency and Accumulated Cyclone Energy, AOGCMs estimated an increase only in  
103 Accumulated Cyclone Energy. Hasegawa and Emori (2007) reported the uncoupled MIROC 3.2  
104 model simulated 6.6% more North Atlantic TCP than its coupled model with fixed anthropogenic  
105 forcing in 1900. After doubling CO<sub>2</sub> from its 1900 level, the uncoupled model predicted increased  
106 TCP (10.4%), but the coupled model yielded a negligible change (0.6%). Yet, the influence of  
107 ocean coupling on the representation and projection of TCP remains poorly characterized,  
108 especially with multi-model ensembles and state-of-the-art GCMs.

109  
110 The High Resolution Model Intercomparison Project (HighResMIP; Haarsma et al., 2016)  
111 provides a unique opportunity to examine the impact of ocean coupling on simulated and projected  
112 TCP. HighResMIP conducted both AGCM and AOGCM experiments with the same set of GCMs,  
113 different horizontal resolutions (varying from 150 to 25 km), and time-varying external forcings  
114 spanning 1950–2050 (Haarsma et al., 2016). Its outputs have been used to investigate global TC  
115 activity with both AGCMs and AOGCMs (Roberts et al., 2020a; Roberts et al., 2020b), as well as  
116 global land precipitation and TCP based on the AGCMs (Bador et al., 2020; Zhang, W., et al.,  
117 2021). Nevertheless, assessing the effect of ocean coupling on TCP is still lacking. Therefore, we  
118 address the following questions: 1) How does the representation of TCP differ in the HighResMIP  
119 AGCM and AOGCM simulations? 2) What physical processes are responsible for any TCP  
120 differences? 3) How does ocean coupling affect projections of future TCP? We first compared the  
121 differences in simulated TCP over 1950–2014 between the AOGCMs and AGCMs in low- and  
122 high-resolutions, and evaluated their performance relative to observations. Then we quantified the

123 impacts of two ocean coupling features (large-scale SST biases and local SST feedback to TCs)  
124 on simulated TCP. Lastly, we assessed projected changes in TCP during 2015–2050 (relative to  
125 1950–2014) and associated uncertainties due to ocean coupling.

126

## 127 **2. Data and methods**

### 128 **2.1. Climate model simulations**

129 Climate model simulations are derived from the HighResMIP (Haarsma et al., 2016), one of the  
130 Model Intercomparison Projects endorsed by the Coupled Model Intercomparison Project Phase 6  
131 (CMIP6). Table S1 describes four different GCMs used in this study, including CMCC-CM2  
132 (Cherchi et al., 2019), CNRM-CM6.1 (Voldoire et al., 2019), EC-Earth3P (Haarsma et al., 2020),  
133 and HadGEM3-GC3.1 (Roberts et al., 2019). This multi-model ensemble was produced by the  
134 European Union Horizon 2020 project PRIMAVERA which follows the HighResMIP protocol at  
135 both a CMIP6 standard (~100 km) and a high (25–50 km) horizontal resolution (Roberts et al.,  
136 2020a). Note that the remaining two GCMs (ECMWF and MPI-M) in the PRIMAVERA were not  
137 included in this study because of incomplete data (e.g., SST) available in the archive. The modeling  
138 centers listed in Table S1 conducted both AGCM (uncoupled) and AOGCM (coupled) simulations  
139 spanning 1950–2050 which covers historical (1950–2014) and future (2015–2050) periods. Details  
140 about the simulation design are described in Haarsma et al. (2016) and Roberts et al. (2020a) and  
141 summarized in the supplemental Text S1.

142

143 Simulated TC tracks were identified using two feature-tracking algorithms, TempestExtremes  
144 (Ullrich & Zarzycki, 2017) and TRACK (Hodges et al., 2017). They can be accessed through the  
145 Centre for Environmental Data Analysis (Roberts 2019a, 2019b). While both algorithms use  
146 criteria for warm-core and lifetime, their primary feature-tracking variables are different (sea level  
147 pressure in TempestExtremes and relative vorticity in TRACK). Characteristics of the  
148 HighResMIP-based TC tracks were summarized in Roberts et al. (2020a, 2020b). For the sake of  
149 brevity, we only discuss the results based on the TRACK algorithm in section 3, which was  
150 available for a greater number of models than the TempestExtremes tracks. The results from the  
151 TempestExtremes algorithm are described in the supplement (Figures S4 & S5), and the findings  
152 based on the two algorithms are similar.

153

## 154 **2.2. Tropical cyclone and precipitation observations**

155 To evaluate the performance of the GCMs, we compared the simulated TCP to observations from  
156 the Tropical Rainfall Measuring Mission (TRMM) dataset which integrates precipitation estimates  
157 from satellites and rain gauge analyses (Huffman et al., 2007). The dataset is chosen to validate  
158 the HighResMIP simulations because of its high temporal (3 hourly in the 3B42 subset) and spatial  
159 resolutions ( $0.25^\circ \times 0.25^\circ$ ) covering  $50^\circ\text{N}$ – $50^\circ\text{S}$  (Huffman et al., 2007; TRMM, 2011). Given the  
160 spatial coverage and time length of TRMM data (1998 to present), we compared the HighResMIP  
161 historical simulations with TRMM over only their common 17-year period (1998–2014) and  
162 latitudes south of  $50^\circ\text{N}$  in the Northern Hemisphere.

163  
164 Observed TC tracks in the North Atlantic and eastern North Pacific basins are maintained by the  
165 National Oceanic and Atmospheric Administration (NOAA) National Hurricane Center’s  
166 hurricane database (HURDAT2; Landsea and Franklin, 2013). TC tracks in the western North  
167 Pacific and North Indian basins are documented by the U.S. Navy’s Joint Typhoon Warning Center  
168 (JTWC) best-track database (Chu et al., 2002). Boundaries of the four TC basins in the Northern  
169 Hemisphere are defined in Figure S1.

## 170 171 **2.3. Analysis methods**

172 We computed and compared TCP during the TC season (May–November) in the AOGCM and  
173 AGCM simulations and the TRMM dataset. Here TCP is defined as average precipitation rate  
174 within a 500 km radius of TC center (Knutson et al., 2020). We calculated the percent difference  
175 in TCP ( $\Delta TCP$ ) associated with ocean coupling as in equation (1). To uncover possible causes of  
176 the difference in simulated TCP over 1950–2014, we also analyzed basin-averaged SSTs and TC  
177 minimum sea level pressure (SLP) and near-surface specific humidity (HUSS) within a 500 km  
178 radius of TC position. Differences in SST, SLP, and HUSS between the AOGCMs and AGCMs  
179 were computed from equations (2–4). These climate variables were derived from the GCM outputs  
180 at the 6 hourly frequency to match with TC time steps. In addition, we estimated the percent change  
181 in future TCP relative to the historical period 1950–2014 for each AOGCM/AGCM simulation  
182 (equation 5).

$$183 \quad \Delta TCP = 100 * (TCP_{AOGCM} - TCP_{AGCM}) / TCP_{AGCM} \quad (1)$$

$$184 \quad \Delta SLP = SLP_{AOGCM} - SLP_{AGCM} \quad (2)$$

185 
$$\Delta HUSS = HUSS_{AOGCM} - HUSS_{AGCM} \quad (3)$$

186 
$$SST \text{ bias} = SST_{AOGCM} - SST_{AGCM} \quad (4)$$

187 
$$\text{Future change in TCP} = 100 * (TCP_{GCM,2015-2050} - TCP_{GCM,1950-2014}) / TCP_{GCM,1950-2014}$$
  
 188 
$$\quad (5)$$

189 
$$\delta SST = SST_{GCM,post-TC} - SST_{GCM,pre-TC} \quad (6)$$

190

191 To quantify TC–ocean interactions in the simulations, we calculated the amplitude of cold wakes  
 192  $\delta SST$  in each AOGCM or AGCM (equation 6). It is defined as the difference between post-TC (1–  
 193 4 days after TC passage) SST and pre-TC (3–10 days before TC passage) SST averaged over a  
 194 200 km radius around each TC position (Vincent et al., 2012a). We note that not all modeling  
 195 centers provide SSTs in their data archive, but surface upwelling longwave radiation is provided.  
 196 When SSTs were not available, we derived SSTs from longwave radiation using the Stefan-  
 197 Boltzmann law. We find no significant difference in cold wakes whether quantified using SST or  
 198 longwave radiation, as demonstrated by the GCMs (HadGEM3-GC3.1 and CMCC-CM2) that  
 199 have both SSTs and surface upwelling longwave radiation available in their data archive (not  
 200 shown).

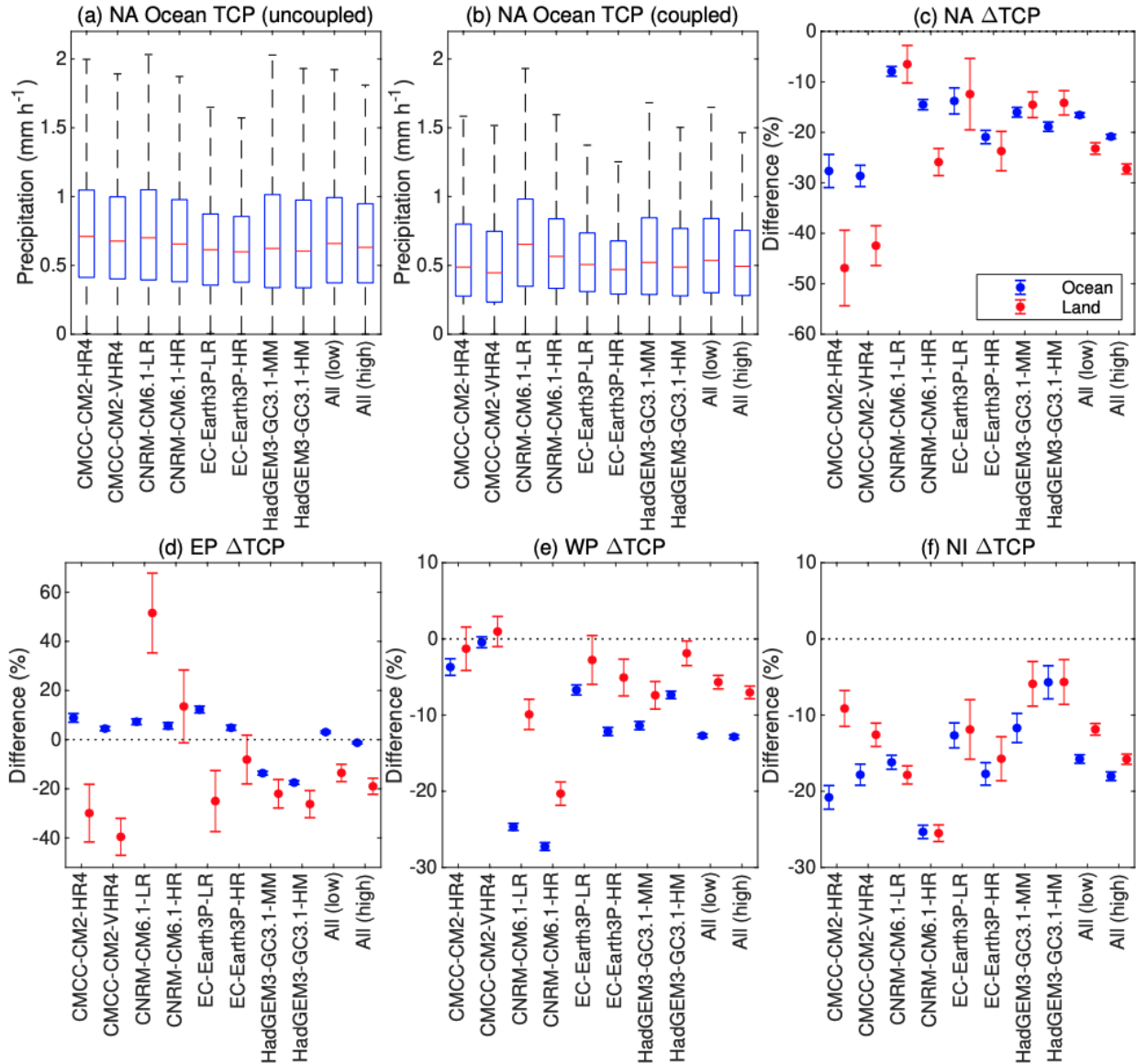
201

### 202 **3. Results and discussion**

#### 203 **3.1. Observed and simulated tropical cyclone precipitation**

204 Simulated TCP during the historical period is relatively insensitive to model resolution, for the  
 205 same AGCM or AOGCM, but the GCMs tend to underestimate TCP compared to the TRMM  
 206 observations. Taking the North Atlantic Ocean as an example, the high- and low-resolution  
 207 AGCMs simulate a median TCP of 0.63 and 0.66 mm h<sup>-1</sup>, respectively (Figure 1a). Their AOGCM  
 208 counterparts yield a median TCP of 0.49 and 0.54 mm h<sup>-1</sup>, respectively (Figure 1b). Like the  
 209 medians, the 95% confidence intervals (CIs) of TCP in the high- and low-resolution simulations  
 210 are very close. Nevertheless, all GCMs (including coupled and uncoupled) underestimate TCP  
 211 compared to the TRMM observations 1998–2014, especially heavy TCP events (Figure S2a, e).  
 212 For example, the uncoupled (coupled) HadGEM3-GC3.1-HM model simulates 24.7% (54.6%)  
 213 less TCP than TRMM over the North Atlantic. Zhang et al. (2019, 2021) also reported  
 214 underestimated TCP, as well as its low sensitivity to model resolution. The undersimulated TCP  
 215 can be attributed to GCMs’ limitation in simulating strong TCs, even with model resolutions as

216 high as 25–50 km (Roberts et al., 2020a). Similar to our findings over the North Atlantic, most of  
 217 the AGCMs and AOGCMs underperform in capturing observed TCP over other TC basins  
 218 (Figures S2 & S3).



219  
 220 **Figure 1.** Boxplots of simulated tropical cyclone precipitation (TCP,  $\text{mm h}^{-1}$ ) from 1950–2014 in  
 221 the (a) uncoupled and (b) coupled simulations by model, and their percentage difference ((coupled  
 222 minus uncoupled) / uncoupled, denoted as  $\Delta\text{TCP}$ ) over the (c) North Atlantic (NA), (d) eastern  
 223 North Pacific (EP), (e) western North Pacific (WP), and (f) North Indian (NI) basins. While  
 224 boxplots in (a–b) are based on TCP over ocean, blue and red error bars in (c–f) represent the  $\Delta\text{TCP}$   
 225 over ocean and land, respectively. The two rightmost boxes in (a–b) or blue/red bars in (c–f) refer  
 226 to the ensemble of all low- and high-resolution model simulations, respectively. The 95%

227 confidence interval in (c–f) is estimated from individually bootstrapping the uncoupled and  
228 coupled data 200 times and then calculating their percentage differences (in relative to the mean  
229 of uncoupled data) and associated bootstrap standard error.

230

### 231 **3.2. The impacts of ocean coupling on tropical cyclone precipitation**

232 Ocean coupling generally leads to decreased TCP over ocean (Figure 1c–f). In the North Atlantic  
233 Ocean, TCP is 7.9–28.6% lower in the eight AOGCMs than in their corresponding AGCMs. The  
234 high-resolution four-member AOGCM ensemble produces 20.8% less TCP than the AGCM  
235 ensemble (95% CI: [-21.3%, -20.4%]). The TCP difference in the low-resolution ensemble is -  
236 16.5% (95% CI: [-17%, -16.1%]), indicating a low sensitivity of TCP difference to model  
237 resolution (Figure 1c). For other ocean basins, we find a similar contrast in TCP arising from ocean  
238 coupling (Figure 1d–f). Specifically, relative to the high-resolution AGCM ensemble, the high-  
239 resolution AOGCM ensemble simulates a difference in TCP of -1.3% (95% CI: [-1.7%, -0.8%])  
240 in the eastern North Pacific, -12.8% (95% CI: [-13.1%, -12.6%]) in the western North Pacific, and  
241 -17.9% (95% CI: [-18.6%, -17.3%]) in the North Indian. The low-resolution AOGCM ensemble  
242 yields comparable TCP, except for the eastern North Pacific (+3.1%). We note that the sign of the  
243 TCP difference over the eastern North Pacific varies by GCM (Figure 1d). While two AOGCMs  
244 (HadGEM3-GC3.1-MM and HadGEM3-GC3.1-HM) simulate 13.6% and 17.5% less TCP,  
245 respectively, the other AOGCMs estimate 4.5–12.3% more TCP, for reasons explained in the  
246 following section.

247

248 Landfalling TCP is likewise decreased with ocean coupling (Figure 1c–f). The high (low)  
249 resolution AOGCM ensemble underestimates landfalling TCP relative to the AGCM ensemble by  
250 -27.2% (-23.2%) in the North Atlantic, -20.4% (-13.4%) in the eastern North Pacific, -6.9% (-  
251 5.5%) in the western North Pacific, and -15.8% (-11.8%) in the North Indian basin. The TCP  
252 differences between the AOGCMs and AGCMs are significantly below 0 at the 0.05 level. Only  
253 one AOGCM (CNRM-CM6.1-LR) simulates significantly higher landfalling TCP (+51.5%) over  
254 the eastern North Pacific basin (Figure 1d). However, the TCP difference simulated by the coupled  
255 CNRM-CM6.1-HR model is not significantly different from 0 (95% CI: [-1.5%, 28.5%]), implying  
256 some uncertainty due to model resolution.

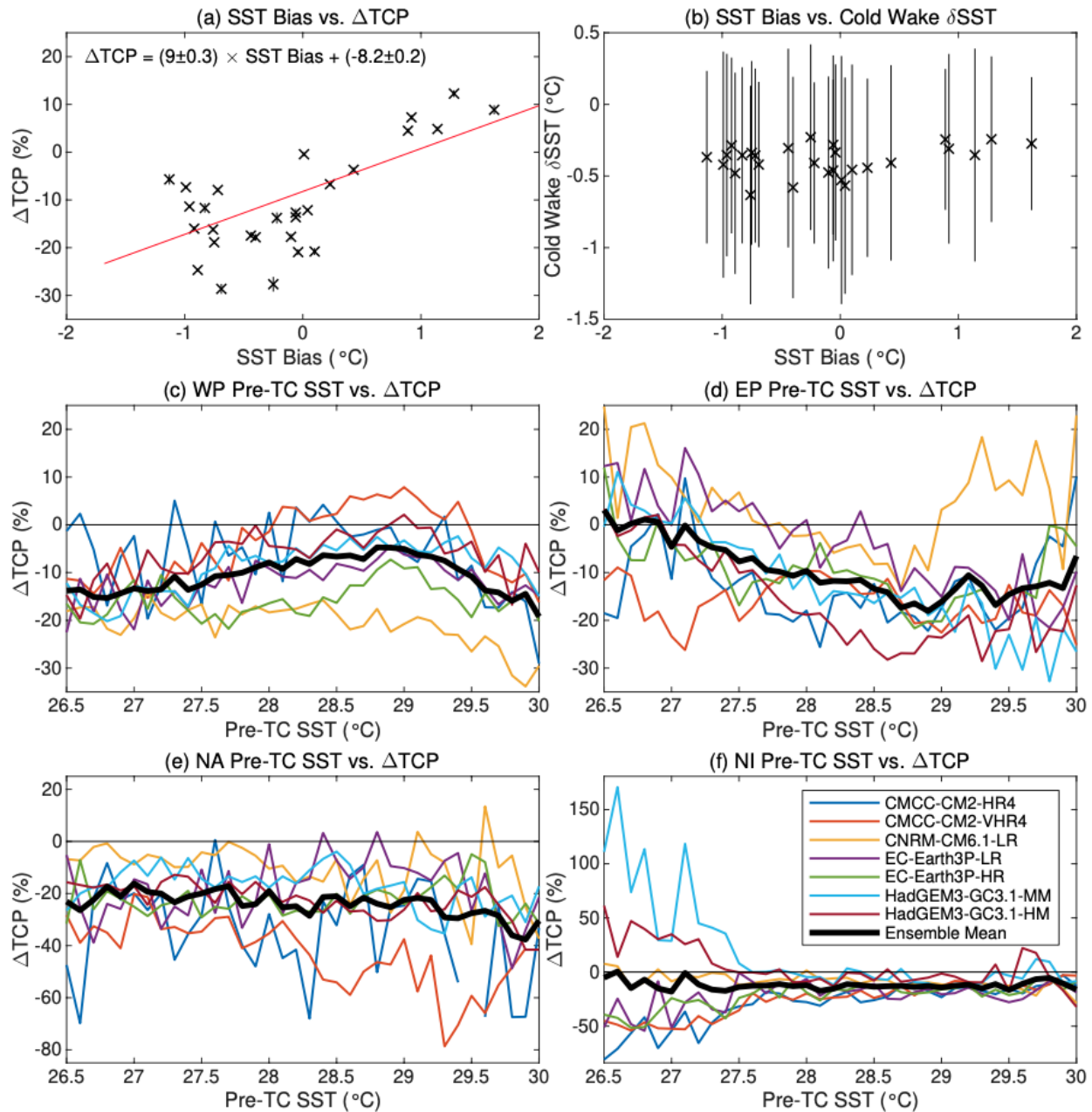
257

### 258 **3.3. The role of large-scale SST biases and TC–ocean feedbacks**

259 Large-scale SST biases of the AOGCMs are critical drivers of the differences in TCP between the  
260 coupled and uncoupled simulations (Figures 2a and S1). Here we characterized large-scale SST  
261 biases as the SST differences between the AOGCMs and prescribed-SSTs AGCMs (i.e.,  
262 observations) over tropical oceans (5–30°N). SST biases are generally cold over the North Atlantic  
263 and North Indian oceans, ranging from -0.92 °C to -0.04 °C and -1.13 °C to 0.1 °C, respectively.  
264 In contrast, SST biases are mostly warm over the eastern North Pacific (except for the HadGEM3-  
265 GC3.1-MM and HadGEM3-GC3.1-HM models) and more mixed in the western North Pacific.  
266 These large-scale SST biases significantly influence the TCP differences between the AOGCMs  
267 and AGCMs (Figure 2a). Their linear regression suggests that every 1 °C of large-scale SST bias  
268 increases TCP by  $9\pm 0.3\%$  in the AOGCMs relative to the AGCMs. Interestingly, AOGCMs and  
269 AGCMs with the same large-scale SST (i.e., zero bias in the AOGCM) produce TCP that differs  
270 by  $-8.2\pm 0.2\%$ . This indicates the importance of some additional mechanism for TCP, potentially  
271 local-scale coupling and TC cold wakes.

272  
273 Therefore, to investigate the potential influence of local-scale SST on TCP, we pose the question:  
274 Given the same local SSTs (averaged within a 200 km radius of each TC center) in the AOGCMs  
275 and AGCMs, do AOGCMs tend to simulate weaker TCP than AGCMs? By comparing TCP with  
276 the same underlying SST, we attempt to evaluate the influence of local-scale SST when controlling  
277 for the existence of large-scale SST biases. Figure 2c–f shows ocean TCP differences against pre-  
278 TC SSTs in the AOGCMs and AGCMs. Here the pre-TC (3–10 days before TC passage) SSTs are  
279 used in order to minimize the impact of TC–ocean interactions on subsequent TCP in the  
280 AOGCMs. We confirm the AOGCMs usually produce lower TCP than their corresponding  
281 AGCMs over warm ocean water ( $SST > 26.5$  °C, a critical SST threshold for TC development in  
282 the current climate; Tory & Dare, 2015). The reduced TCP in the AOGCMs relative to AGCMs is  
283 evident in a vast majority of the models, SST ranges, and ocean basins. We caution that over part  
284 of the North Indian Ocean where SSTs are below 27.5 °C, there are large positive TCP differences  
285 in the HadGEM3-GC3.1-MM and HadGEM3-GC3.1-HM models, because TCP in their AGCM  
286 simulations is much lower than those in the AOGCM runs (Figure 2f). But the TCP differences  
287 become negative with warmer water ( $> 27.5$  °C), in line with other GCMs and basins.

288



289  
 290 **Figure 2.** (a) Basin-scale SST bias ( $^{\circ}\text{C}$ ) averaged over tropical oceans ( $5\text{--}30^{\circ}\text{N}$ ) from the AOGCM  
 291 and the percentage difference in ocean tropical cyclone (TC) precipitation ( $\Delta\text{TCP}$ ) between the  
 292 coupled and uncoupled simulations during the period from May to November 1950–2014. (b)  
 293 Basin-scale SST bias and TC cold wake  $\delta\text{SST}$  ( $^{\circ}\text{C}$ ) in the coupled simulations. (c–f) Ocean-  
 294 specific  $\Delta\text{TCP}$  with the same pre-TC SST (binned by  $0.1^{\circ}\text{C}$  increment) in the coupled and  
 295 uncoupled simulations. Each point in (a–b) is derived from a unique combination of four ocean  
 296 basins and seven climate models (SST data is not available in the CNRM-CM6.1-HR model), with  
 297 the error bar in y-axis representing its uncertainty range (mean  $\pm$  one standard deviation).

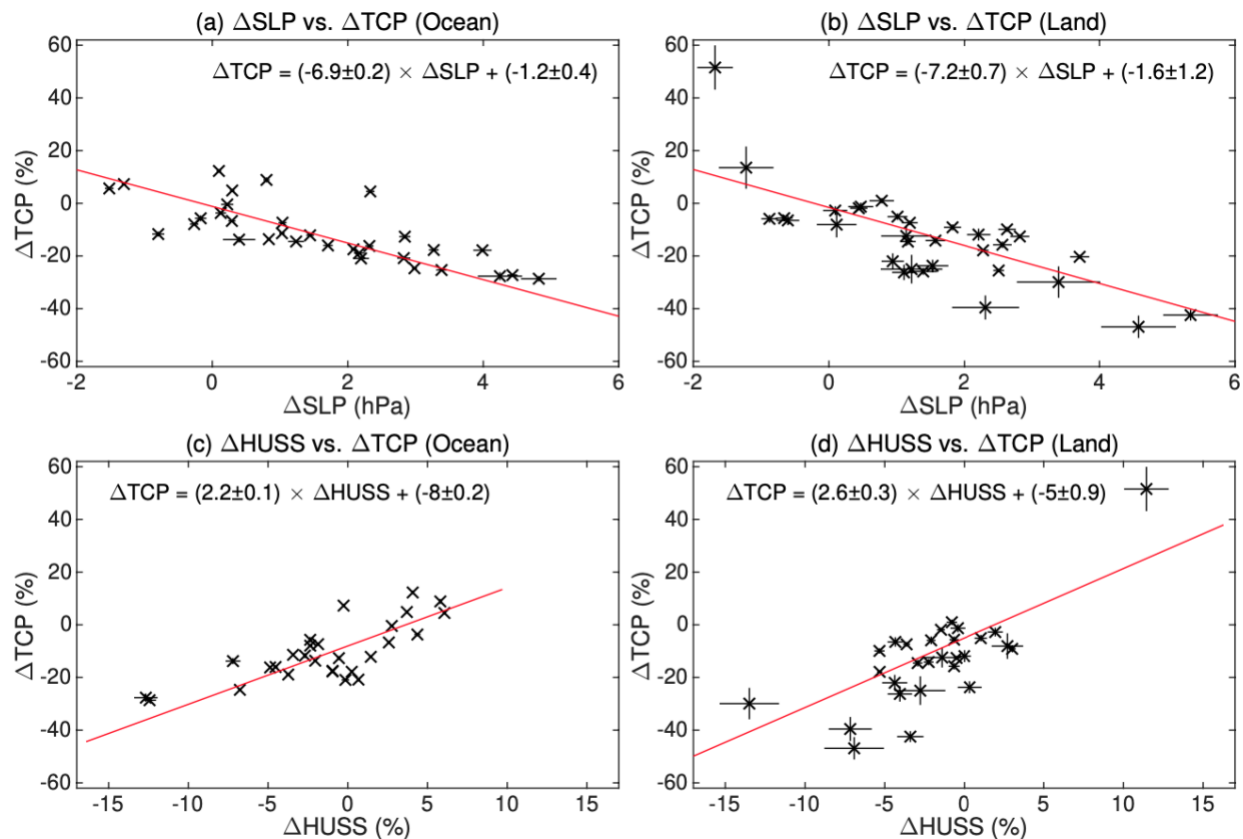
298

299 Given absent large-scale SST bias and similar local pre-TC SSTs, what physical processes in the  
300 AOGCMs may be responsible for the weaker TCP compared to AGCMs? Past studies have linked  
301 TC-induced cold wakes to suppressed TC intensity and reduced post-TC precipitation (Karnauskas  
302 et al., 2021; Ma et al., 2020). By contrasting SST changes before and after TC passage in both the  
303 AOGCMs and AGCMs, we evaluated the impacts of TC cold wakes on TCP and TC intensity.  
304 Figure 2b shows that TCs in the AOGCMs do produce appreciable cold wakes, regardless of large-  
305 scale SST biases. The magnitudes of cold wakes are averaged at -0.63 to -0.23 °C among all ocean  
306 basins and AOGCMs. The more intense TCs tend to produce stronger cold wakes (not shown).  
307 We note the magnitudes of simulated cold wakes are smaller than those in observations (Vincent  
308 et al., 2012a), because the GCMs tend to generate weaker TCs than observations (Roberts et al.,  
309 2020a). As expected, TCs in the AGCMs do not generate cold wakes (not shown), since SSTs are  
310 prescribed from observations as per the HighResMIP protocol (Haarsma et al., 2016). In other  
311 words, the AOGCMs reproduce active atmosphere–ocean interactions which result in local and  
312 negative SST feedback to TCs via cold wakes, but the AGCMs do not. The interactions and  
313 feedback have been found to modulate enthalpy flux and regional atmospheric circulation, and  
314 therefore negatively affect TC intensity and precipitation (Karnauskas et al., 2021; Kushnir et al.,  
315 2002; Ma et al., 2020; Trenberth et al., 1998; Vincent et al., 2012b; Zarzycki, 2016). We find  
316 generally decreased TCP in the AOGCMs, in the absence of large-scale SST bias and with similar  
317 local pre-TC SSTs. This is in agreement with previous studies on TC-related precipitation  
318 (Hasegawa & Emori, 2007; Ma et al., 2020). Our findings suggest that cold wakes may play an  
319 important role in decreasing TCP, independent of the contributions from large-scale SST biases.

320

321 Large-scale SST biases and TC cold wakes, both tied to ocean coupling in the AOGCMs, influence  
322 TCP in association with changes in sea level pressure and specific humidity. Figure 3 compares  
323 the difference between AOGCM and AGCM TC minimum sea level pressure and near-surface  
324 specific humidity. We discover that TC minimum sea level pressure over both ocean and land is  
325 typically higher in the AOGCMs compared to AGCMs (Figure 3a–b), which means weaker TC  
326 intensity. Specific humidity is lower in most AOGCMs (Figure 3c–d). Furthermore, both sea level  
327 pressure and specific humidity are linearly correlated ( $p < 0.01$ ) with the difference in TCP.

328



329  
 330 **Figure 3.** Differences in TC minimum sea level pressure ( $\Delta$ SLP, hPa), near-surface specific  
 331 humidity ( $\Delta$ HUSS, %), and tropical cyclone precipitation ( $\Delta$ TCP, %) between the coupled and  
 332 uncoupled simulations over ocean (a, c) and land (b,d). Each point is derived from a unique  
 333 combination of four ocean basins and seven/eight climate models ( $\Delta$ HUSS data is not available in  
 334 the CNRM-CM6.1-HR model), with the error bar representing its uncertainty range (mean  $\pm$  one  
 335 standard deviation).

336  
 337 To sum up, large-scale SST biases primarily drive the TCP difference between the AOGCMs and  
 338 AGCMs, and local TC–ocean feedbacks via SST cold wakes in the AOGCMs reinforce the TCP  
 339 contrast. The dynamic and thermodynamic processes through which they are linked include  
 340 weakened TC intensity and decreased specific humidity in most ocean basins and AOGCMs.  
 341 Given the design of the HighResMIP AGCM and AOGCM experiments, it is very difficult to  
 342 completely isolate the effects of large-scale SST biases and cold wakes on the processes and  
 343 therefore TCP. A better understanding of their individual effects warrants a further study, such as  
 344 running AGCM-like experiments with TC cold wakes specified (Karnauskas et al., 2021) or

345 mechanistic experiments based on specific TC events using a simple ocean model that lacks basin-  
346 scale SST biases, as suggested by Patricola & Wehner (2018).

347

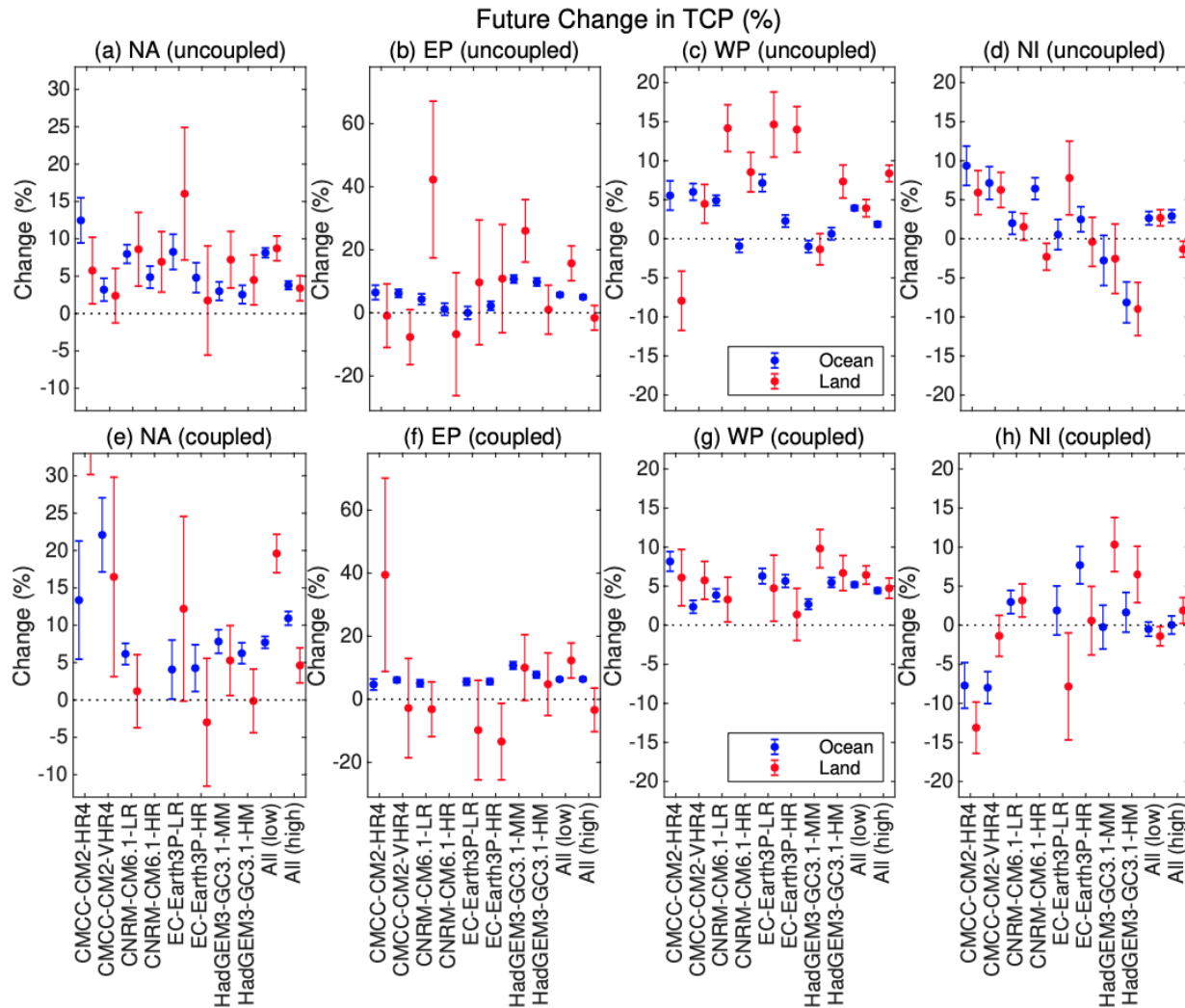
### 348 **3.4. Projected tropical cyclone precipitation and its dependence on ocean coupling**

349 The AOGCMs and AGCMs consistently predict an increase in ocean TCP during 2015–2050  
350 relative to 1950–2014 across all TC basins (Figure 4). The high-resolution AGCM (AOGCM)  
351 ensemble projects TCP to increase by 3.7% (10.9%) in the North Atlantic, 5.0% (6.5%) in the  
352 eastern North Pacific, 1.8% (4.4%) in the western North Pacific, and 3.0% (0.2%) in the North  
353 Indian oceans. The increases in ocean TCP are significant at 0.05 level, because their 95% CIs are  
354 generally above 0 (except for the AOGCMs runs in the North Indian Ocean). The low-resolution  
355 GCMs produce similar changes, despite intermodel differences in their magnitudes.

356

357 Landfalling TCP is expected to increase in the North Atlantic and western North Pacific basins,  
358 whereas TCP changes in the eastern North Pacific and North Indian basins are mixed (Figure 4).  
359 The high-resolution AGCM (AOGCM) ensemble predicts landfalling TCP to rise by 4.2% (4.5%)  
360 and 8.3% (5.0%) over the North Atlantic and western North Pacific basins, respectively. These  
361 increases are significant at the 0.05 level, as are the changes simulated by the low-resolution  
362 GCMs. In the eastern North Pacific, however, landfalling TCP is projected to decrease by 1.7%  
363 (1.9%) in the high-resolution AGCM (AOGCM) ensemble, although the changes are insignificant.  
364 Conversely, the low-resolution AGCM (AOGCM) ensemble estimates a substantial TCP  
365 intensification of 16.9% (11.4%). Over the North Indian basin, landfalling TCP is expected to  
366 decrease (increase) significantly by 1.2% (2.3%) in the high-resolution AGCMs (AOGCMs). The  
367 low-resolution AGCMs and AOGCMs yield changes of 2.7% and -1.2%, respectively. The  
368 opposite changes demonstrate a large uncertainty in landfalling TCP predictions over the eastern  
369 North Pacific and North Indian basins. In summary, future TCP over land and ocean is generally  
370 predicted to increase, with a few exceptions for individual GCMs and basins. The magnitude of  
371 the TCP changes can vary by a factor of 3 depending on whether the ocean is coupled with the  
372 atmosphere, for example for North Atlantic TCs over ocean in the high-resolution simulations.  
373 Our findings align with Knutson et al. (2020), Scoccimarro et al. (2014), and Patricola & Wehner  
374 (2018) who discovered robust increases in TCP with future anthropogenic warming.

375



376  
 377 **Figure 4.** Percentage changes in 2015–2050 tropical cyclone precipitation relative to 1950–2014  
 378 by model and basin in the (a–d) uncoupled and (e–h) coupled simulations. Blue and red error bars  
 379 in each panel represent future changes in TCP over ocean and land, respectively. The basins  
 380 include the North Atlantic (NA), eastern North Pacific (EP), western North Pacific (WP), and  
 381 North Indian (NI). The two rightmost blue/red bars in each panel refer to the ensemble of all low-  
 382 and high-resolution model simulations, respectively. The 95% confidence interval is estimated  
 383 from individually bootstrapping the 2015–2050 and 1950–2014 data 200 times and then  
 384 calculating their percentage differences (in relative to the mean of 1950–2014 data) and associated  
 385 bootstrap standard error. The first red error bar in (e) extends beyond the figure because of its large  
 386 uncertainty in the future change in TCP.

387

#### 388 4. Conclusions

389 This study aims to quantify the impacts of ocean coupling — associated with basin-scale SST  
390 biases and local-scale TC–ocean feedbacks — on simulated and projected TCP in the Northern  
391 Hemisphere. We find that ocean coupling generally leads to decreased TCP during 1950–2014  
392 over ocean and land. The TCP difference exhibits a low sensitivity to model resolution across TC  
393 basins (except the eastern North Pacific). Large-scale SST biases in the AOGCMs are critical  
394 drivers of the TCP difference. Every 1 °C of large-scale SST bias increases TCP by  $9\pm 0.3\%$  in the  
395 AOGCMs relative to the AGCMs. Moreover, local TC–ocean feedbacks via SST cold wakes also  
396 play an important role in decreasing TCP in the AOGCMs, as demonstrated by the TCP decline  
397 with the absence of large-scale SST biases. Both large-scale SST biases and cold wakes are present  
398 due to ocean coupling in the AOGCMs. Altogether the two features influence TCP by modulating  
399 its sea level pressure and specific humidity, with decreased TCP in the AOGCMs associated with  
400 higher sea level pressure (i.e., weaker TC intensity) and lower humidity. During the future period  
401 of 2015–2050, TCP over ocean is projected to increase across all TC basins, consistent in the  
402 AOGCMs and AGCMs, although the magnitude can vary by up to a factor of 3 depending on  
403 whether the ocean is coupled. Landfalling TCP will likewise increase in the North Atlantic and  
404 western North Pacific basins, but TCP changes over the eastern North Pacific and North Indian  
405 basins are mixed. Our findings highlight the importance of better understanding and characterizing  
406 the physical mechanisms governing the accurate representations of SSTs, TCs, and TCP. Bridging  
407 the gap between AOGCMs and AGCMs may provide a better constraint on future TCP projections,  
408 and therefore a more robust assessment of future climate change risk.

409  
410

### 411 **Acknowledgements**

412 This material is based upon work supported by the U.S. Department of Energy, Office of Science,  
413 Office of Biological and Environmental Research, Climate and Environmental Sciences Division,  
414 Regional & Global Model Analysis Program, under Award Number DE-AC02-05CH11231. CMP  
415 acknowledges support from the U.S. Department of Energy, Office of Science, Office of  
416 Biological and Environmental Research (BER), Earth and Environmental Systems Modeling  
417 (EESM) Program, under Early Career Research Program Award Number DE-SC0021109. This  
418 research used resources of the National Energy Research Scientific Computing Center (NERSC),  
419 a U.S. Department of Energy Office of Science User Facility operated under Contract No. DE-

420 AC02-05CH11231. We thank the modeling groups within PRIMAVERA (a European Union  
421 Horizon 2020 project under Grant Agreement 641727) for producing the multi-model simulations  
422 and providing the climate model outputs via the Earth System Grid Federation (ESGF). We greatly  
423 appreciate Malcolm Roberts and Jon Seddon (UK Met Office Hadley Centre) for their help in  
424 accessing the model data through the UK Centre for Environmental Data Analysis's JASMIN  
425 platform.

426

427

### 428 **Data Availability Statement**

429 The climate datasets and tropical cyclone (TC) tracks used in this work are publicly available, with  
430 their DOIs/links cited in this manuscript. The HighResMIP-PRIMAVERA climate model outputs  
431 are available on the Earth System Grid Federation nodes ([https://esgf-](https://esgf-index1.ceda.ac.uk/search/cmip6-ceda)  
432 [index1.ceda.ac.uk/search/cmip6-ceda](https://esgf-index1.ceda.ac.uk/search/cmip6-ceda)) under references Scoccimarro et al. (2017a, 2017b),  
433 Voldoire (2019a, 2019b), EC-Earth Consortium (2019a, 2019b), and Roberts (2017a, 2017b). The  
434 model data can also be accessed at the UK Centre for Environmental Data Analysis's JASMIN  
435 platform (<https://www.ceda.ac.uk/services/jasmin/>). Simulated TC tracks can be accessed through  
436 the UK Centre for Environmental Data Analysis under references Roberts (2019a, 2019b).  
437 Observed TC tracks in the North Atlantic and eastern North Pacific basins are obtained from  
438 NOAA National Hurricane Center (<https://www.nhc.noaa.gov/data/#hurdat>). Observed TC tracks  
439 in the western North Pacific and North Indian basins are obtained from the U.S. Navy's Joint  
440 Typhoon Warning Center (<https://www.metoc.navy.mil/jtwc/jtwc.html?best-tracks>). The Tropical  
441 Rainfall Measuring Mission (TRMM) dataset is accessed from NASA's Goddard Earth Sciences  
442 Data and Information Services Center (<https://doi.org/10.5067/TRMM/TMPA/3H/7>).

443

444

### 445 **Conflict of Interest**

446 There is no financial conflict of interest for any author.

447

448

### 449 **References**

450 Bador, M., Boé, J., Terray, L., Alexander, L. V., Baker, A., Bellucci, A., et al. (2020). Impact of

451 higher spatial atmospheric resolution on precipitation extremes over land in global climate  
452 models. *Journal of Geophysical Research: Atmospheres*.  
453 <https://doi.org/10.1029/2019jd032184>

454 Bakkensen, L. A., Park, D. S. R., & Sarkar, R. S. R. (2018). Climate costs of tropical cyclone  
455 losses also depend on rain. *Environmental Research Letters*, *13*(7), 074034.  
456 <https://doi.org/10.1088/1748-9326/aad056>

457 Bell, J. E., Brown, C. L., Conlon, K., Herring, S., Kunkel, K. E., Lawrimore, J., et al. (2018).  
458 Changes in extreme events and the potential impacts on human health. *Journal of the Air &*  
459 *Waste Management Association*, *68*(4), 265–287.  
460 <https://doi.org/10.1080/10962247.2017.1401017>

461 Centre for Research on the Epidemiology of Disasters (CRED). (2021). EM-DAT | The  
462 international disasters database. Retrieved from <https://www.emdat.be/>

463 Cherchi, A., Fogli, P. G., Lovato, T., Peano, D., Iovino, D., Gualdi, S., et al. (2019). Global mean  
464 climate and main patterns of variability in the CMCC-CM2 coupled model. *Journal of*  
465 *Advances in Modeling Earth Systems*, *11*(1), 2018MS001369.  
466 <https://doi.org/10.1029/2018MS001369>

467 Chu, J. H., C. R. Sampson, A. S. Levine, and E. F. (2002). The Joint Typhoon Warning Center  
468 Tropical Cyclone Best-Tracks, 1945-2000. Retrieved from  
469 <https://www.metoc.navy.mil/jtwc/products/best-tracks/tc-bt-report.html>

470 EC-Earth Consortium. (2019a). EC-Earth-Consortium EC-Earth3P-HR model output prepared  
471 for CMIP6 HighResMIP. <https://doi.org/10.22033/ESGF/CMIP6.2323>

472 EC-Earth Consortium. (2019b). EC-Earth-Consortium EC-Earth3P model output prepared for  
473 CMIP6 HighResMIP. <https://doi.org/10.22033/ESGF/CMIP6.2322>

474 Eyring, V., Bony, S., Meehl, G. A., Senior, C. A., Stevens, B., Stouffer, R. J., & Taylor, K. E.  
475 (2016). Overview of the Coupled Model Intercomparison Project Phase 6 (CMIP6)  
476 experimental design and organization. *Geoscientific Model Development*, *9*(5), 1937–1958.  
477 <https://doi.org/10.5194/gmd-9-1937-2016>

478 Haarsma, R., Acosta, M., Bakhshi, R., Bretonnière, P. A., Caron, L. P., Castrillo, M., et al.  
479 (2020). HighResMIP versions of EC-Earth: EC-Earth3P and EC-Earth3P-HR - Description,  
480 model computational performance and basic validation. *Geoscientific Model Development*,  
481 *13*(8), 3507–3527. <https://doi.org/10.5194/gmd-13-3507-2020>

482 Haarsma, R. J., Roberts, M. J., Vidale, P. L., Catherine, A., Bellucci, A., Bao, Q., et al. (2016).  
483 High Resolution Model Intercomparison Project (HighResMIP v1.0) for CMIP6.  
484 *Geoscientific Model Development*. <https://doi.org/10.5194/gmd-9-4185-2016>

485 Hasegawa, A., & Emori, S. (2007). Effect of air-sea coupling in the assessment of CO<sub>2</sub>-induced  
486 intensification of tropical cyclone activity. *Geophysical Research Letters*.  
487 <https://doi.org/10.1029/2006GL028275>

488 Hodges, K., Cobb, A., & Vidale, P. L. (2017). How well are tropical cyclones represented in  
489 reanalysis datasets? *Journal of Climate*. <https://doi.org/10.1175/JCLI-D-16-0557.1>

490 Hsu, W. C., Patricola, C. M., & Chang, P. (2019). The impact of climate model sea surface  
491 temperature biases on tropical cyclone simulations. *Climate Dynamics*, 53(1–2), 173–192.  
492 <https://doi.org/10.1007/s00382-018-4577-5>

493 Huffman, G. J., Adler, R. F., Bolvin, D. T., Gu, G., Nelkin, E. J., Bowman, K. P., et al. (2007).  
494 The TRMM Multisatellite Precipitation Analysis (TMPA): Quasi-global, multiyear,  
495 combined-sensor precipitation estimates at fine scales. *Journal of Hydrometeorology*.  
496 <https://doi.org/10.1175/JHM560.1>

497 Karnauskas, K. B., Zhang, L., & Emanuel, K. A. (2021). The Feedback of Cold Wakes on  
498 Tropical Cyclones. *Geophysical Research Letters*, 48(7), e2020GL091676.  
499 <https://doi.org/10.1029/2020GL091676>

500 Kennedy, John; Titchner, Holly; Rayner, Nick; Roberts, M. (2017).  
501 input4MIPs.MOHC.SSTsAndSeaIce.HighResMIP.MOHC-HadISST-2-2-0-0-0.  
502 <https://doi.org/10.22033/ESGF/input4MIPs.1221>

503 Knutson, T., Camargo, S. J., Chan, J. C. L., Emanuel, K., Ho, C. H., Kossin, J., et al. (2020).  
504 Tropical cyclones and climate change assessment part II: Projected response to  
505 anthropogenic warming. *Bulletin of the American Meteorological Society*, 101(3), E303–  
506 E322. <https://doi.org/10.1175/BAMS-D-18-0194.1>

507 Kushnir, Y., Robinson, W. A., Bladé, I., Hall, N. M. J., Peng, S., & Sutton, R. (2002).  
508 Atmospheric GCM response to extratropical SST anomalies: Synthesis and evaluation.  
509 *Journal of Climate*, 15(16), 2233–2256. [https://doi.org/10.1175/1520-0442\(2002\)015<2233:AGRTES>2.0.CO;2](https://doi.org/10.1175/1520-0442(2002)015<2233:AGRTES>2.0.CO;2)

511 Landsea, C. W., & Franklin, J. L. (2013). Atlantic Hurricane Database Uncertainty and  
512 Presentation of a New Database Format. *Monthly Weather Review*, 141(10), 3576–3592.

513 <https://doi.org/10.1175/MWR-D-12-00254.1>

514 Li, H., & Sriver, R. L. (2018). Tropical Cyclone Activity in the High-Resolution Community  
515 Earth System Model and the Impact of Ocean Coupling. *Journal of Advances in Modeling*  
516 *Earth Systems*. <https://doi.org/10.1002/2017MS001199>

517 Li, H., & Sriver, R. L. (2019). Impact of air–sea coupling on the simulated global tropical  
518 cyclone activity in the high-resolution Community Earth System Model (CESM). *Climate*  
519 *Dynamics*. <https://doi.org/10.1007/s00382-019-04739-8>

520 Liu, J., Curry, J. A., Clayson, C. A., & Bourassa, M. A. (2011). High-resolution satellite surface  
521 latent heat fluxes in North Atlantic hurricanes. *Monthly Weather Review*, 139(9), 2735–  
522 2747. <https://doi.org/10.1175/2011MWR3548.1>

523 Ma, Z., Fei, J., Lin, Y., & Huang, X. (2020). Modulation of Clouds and Rainfall by Tropical  
524 Cyclone’s Cold Wakes. *Geophysical Research Letters*, 47(17), e2020GL088873.  
525 <https://doi.org/10.1029/2020GL088873>

526 Mendelsohn, R., Emanuel, K., Chonabayashi, S., & Bakkensen, L. (2012). The impact of climate  
527 change on global tropical cyclone damage. *Nature Climate Change*, 2(3), 205–209.  
528 <https://doi.org/10.1038/nclimate1357>

529 NOAA National Centers for Environmental Information. (2021). Billion-Dollar Weather and  
530 Climate Disasters: Overview | National Centers for Environmental Information (NCEI).  
531 Retrieved from <https://www.ncdc.noaa.gov/billions/>

532 O’Neill, B. C., Tebaldi, C., Van Vuuren, D. P., Eyring, V., Friedlingstein, P., Hurtt, G., et al.  
533 (2016). The Scenario Model Intercomparison Project (ScenarioMIP) for CMIP6.  
534 *Geoscientific Model Development*, 9(9), 3461–3482. [https://doi.org/10.5194/gmd-9-3461-](https://doi.org/10.5194/gmd-9-3461-2016)  
535 2016

536 Patricola, C. M., & Wehner, M. F. (2018). Anthropogenic influences on major tropical cyclone  
537 events. *Nature*, 563(7731), 339–346. <https://doi.org/10.1038/s41586-018-0673-2>

538 Poli, P., Hersbach, H., Dee, D. P., Berrisford, P., Simmons, A. J., Vitart, F., et al. (2016). ERA-  
539 20C: An atmospheric reanalysis of the twentieth century. *Journal of Climate*, 29(11), 4083–  
540 4097. <https://doi.org/10.1175/JCLI-D-15-0556.1>

541 Price, J. F. (1981). *Upper ocean response to a hurricane. Upper ocean response to a hurricane.*  
542 Woods Hole Oceanographic Institution. <https://doi.org/10.1575/1912/10271>

543 Rappaport, E. N. (2014). Fatalities in the united states from atlantic tropical cyclones: New data

544 and interpretation. *Bulletin of the American Meteorological Society*, 95(3), 341–346.  
545 <https://doi.org/10.1175/BAMS-D-12-00074.1>

546 Rappaport, E. N., & Blanchard, B. W. (2016, July 1). Fatalities in the United States indirectly  
547 associated with Atlantic tropical cyclones. *Bulletin of the American Meteorological Society*.  
548 American Meteorological Society. <https://doi.org/10.1175/BAMS-D-15-00042.1>

549 Richter, I. (2015). Climate model biases in the eastern tropical oceans: causes, impacts and ways  
550 forward. *Wiley Interdisciplinary Reviews: Climate Change*, 6(3), 345–358.  
551 <https://doi.org/10.1002/wcc.338>

552 Richter, I., & Tokinaga, H. (2020). An overview of the performance of CMIP6 models in the  
553 tropical Atlantic: mean state, variability, and remote impacts. *Climate Dynamics*, 55(9–10),  
554 2579–2601. <https://doi.org/10.1007/s00382-020-05409-w>

555 Roberts, M. (2017a). MOHC HadGEM3-GC31-HM model output prepared for CMIP6  
556 HighResMIP. <https://doi.org/10.22033/ESGF/CMIP6.446>

557 Roberts, M. (2017b). MOHC HadGEM3-GC31-MM model output prepared for CMIP6  
558 HighResMIP. <https://doi.org/10.22033/ESGF/CMIP6.1902>

559 Roberts, M. J., Baker, A., Blockley, E. W., Calvert, D., Coward, A., Hewitt, H. T., et al. (2019).  
560 Description of the resolution hierarchy of the global coupled HadGEM3-GC3.1 model as  
561 used in CMIP6 HighResMIP experiments. *Geoscientific Model Development*, 12(12), 4999–  
562 5028. <https://doi.org/10.5194/gmd-12-4999-2019>

563 Roberts, M. (2019a). CMIP6 HighResMIP: Tropical storm tracks as calculated by the TRACK  
564 algorithm. Retrieved from  
565 <http://catalogue.ceda.ac.uk/uuid/0b42715a7a804290afa9b7e31f5d7753>

566 Roberts, M. (2019b). CMIP6 HighResMIP: Tropical storm tracks as calculated by the  
567 TempestExtremes algorithm. Retrieved from  
568 <http://catalogue.ceda.ac.uk/uuid/438268b75fed4f27988dc02f8a1d756d>

569 Roberts, M. J., Camp, J., Seddon, J., Vidale, P. L., Hodges, K., Vanniere, B., et al. (2020a).  
570 Impact of model resolution on tropical cyclone simulation using the HighResMIP-  
571 PRIMAVERA multimodel ensemble. *Journal of Climate*. [https://doi.org/10.1175/JCLI-D-](https://doi.org/10.1175/JCLI-D-19-0639.1)  
572 19-0639.1

573 Roberts, M. J., Camp, J., Seddon, J., Vidale, P. L., Hodges, K., Vannière, B., et al. (2020b).  
574 Projected Future Changes in Tropical Cyclones Using the CMIP6 HighResMIP Multimodel

575 Ensemble. *Geophysical Research Letters*. <https://doi.org/10.1029/2020GL088662>

576 Scoccimarro, E., Gualdi, S., Villarini, G., Vecchi, G. A., Zhao, M., Walsh, K., & Navarra, A.  
577 (2014). Intense precipitation events associated with landfalling tropical cyclones in response  
578 to a warmer climate and increased CO<sub>2</sub>. *Journal of Climate*, 27(12), 4642–4654.  
579 <https://doi.org/10.1175/JCLI-D-14-00065.1>

580 Scoccimarro, E., Bellucci, A., & Peano, D. (2017a). CMCC CMCC-CM2-HR4 model output  
581 prepared for CMIP6 HighResMIP. <https://doi.org/10.22033/ESGF/CMIP6.1359>

582 Scoccimarro, E., Bellucci, A., & Peano, D. (2017b). CMCC CMCC-CM2-VHR4 model output  
583 prepared for CMIP6 HighResMIP. <https://doi.org/10.22033/ESGF/CMIP6.1367>

584 Scoccimarro, E., Fogli, P. G., Reed, K. A., Gualdi, S., Masina, S., & Navarra, A. (2017c).  
585 Tropical cyclone interaction with the ocean: The role of high-frequency (subdaily) coupled  
586 processes. *Journal of Climate*, 30(1), 145–162. <https://doi.org/10.1175/JCLI-D-16-0292.1>

587 Tory, K. J., & Dare, R. A. (2015). Sea surface temperature thresholds for tropical cyclone  
588 formation. *Journal of Climate*, 28(20), 8171–8183. <https://doi.org/10.1175/JCLI-D-14-00637.1>

589

590 Trenberth, K. E., Branstator, G. W., Karoly, D., Kumar, A., Lau, N.-C., & Ropelewski, C.  
591 (1998). Progress during TOGA in understanding and modeling global teleconnections  
592 associated with tropical sea surface temperatures. *Journal of Geophysical Research:*  
593 *Oceans*, 103(C7), 14291–14324. <https://doi.org/10.1029/97JC01444>

594 Tropical Rainfall Measuring Mission (TRMM). (2011). TRMM (TMPA) Rainfall Estimate L3 3  
595 hour 0.25 degree x 0.25 degree V7, Greenbelt, MD, Goddard Earth Sciences Data and  
596 Information Services Center (GES DISC). <https://doi.org/10.5067/TRMM/TMPA/3H/7>

597 Ullrich, P. A., & Zarzycki, C. M. (2017). TempestExtremes: A framework for scale-insensitive  
598 pointwise feature tracking on unstructured grids. *Geoscientific Model Development*.  
599 <https://doi.org/10.5194/gmd-10-1069-2017>

600 Vincent, E. M., Lengaigne, M., Madec, G., Vialard, J., Samson, G., Jourdain, N. C., et al.  
601 (2012a). Processes setting the characteristics of sea surface cooling induced by tropical  
602 cyclones. *Journal of Geophysical Research: Oceans*. <https://doi.org/10.1029/2011JC007396>

603 Vincent, E. M., Lengaigne, M., Vialard, J., Madec, G., Jourdain, N. C., & Masson, S. (2012b).  
604 Assessing the oceanic control on the amplitude of sea surface cooling induced by tropical  
605 cyclones. *Journal of Geophysical Research: Oceans*, 117(C5), n/a-n/a.

606 <https://doi.org/10.1029/2011JC007705>

607 Voldoire, A., Saint-Martin, D., S n si, S., Decharme, B., Alias, A., Chevallier, M., et al. (2019).  
608 Evaluation of CMIP6 DECK Experiments With CNRM-CM6-1. *Journal of Advances in*  
609 *Modeling Earth Systems*, 11(7), 2177–2213. <https://doi.org/10.1029/2019MS001683>

610 Voldoire, A. (2019a). CNRM-CERFACS CNRM-CM6-1-HR model output prepared for CMIP6  
611 HighResMIP. <https://doi.org/10.22033/ESGF/CMIP6.1387>

612 Voldoire, A. (2019b). CNRM-CERFACS CNRM-CM6-1 model output prepared for CMIP6  
613 HighResMIP. <https://doi.org/10.22033/ESGF/CMIP6.1925>

614 Walsh, K. J. E., McBride, J. L., Klotzbach, P. J., Balachandran, S., Camargo, S. J., Holland, G.,  
615 et al. (2016). Tropical cyclones and climate change. *Wiley Interdisciplinary Reviews:*  
616 *Climate Change*, 7(1), 65–89. <https://doi.org/10.1002/wcc.371>

617 Wehner, M., Prabhat, Reed, K. A., Stone, D., Collins, W. D., Bacmeister, J., et al. (2015).  
618 Resolution Dependence of Future Tropical Cyclone Projections of CAM5.1 in the U.S.  
619 CLIVAR Hurricane Working Group Idealized Configurations. *Journal of Climate*, 28(10),  
620 3905–3925. <https://doi.org/10.1175/JCLI-D-14-00311.1>

621 Zarzycki, C. M. (2016). Tropical cyclone intensity errors associated with lack of two-way ocean  
622 coupling in high-resolution global simulations. *Journal of Climate*.  
623 <https://doi.org/10.1175/JCLI-D-16-0273.1>

624 Zhang, G., Murakami, H., Yang, X., Findell, K. L., Wittenberg, A. T., & Jia, L. (2021).  
625 Dynamical seasonal predictions of tropical cyclone activity: Roles of sea surface  
626 temperature errors and atmosphere-land initialization. *Journal of Climate*, 34(5), 1743–  
627 1766. <https://doi.org/10.1175/JCLI-D-20-0215.1>

628 Zhang, W., Villarini, G., Vecchi, G. A., & Murakami, H. (2019). Rainfall from tropical cyclones:  
629 high-resolution simulations and seasonal forecasts. *Climate Dynamics*, 52(9–10), 5269–  
630 5289. <https://doi.org/10.1007/s00382-018-4446-2>

631 Zhang, W., Villarini, G., Scoccimarro, E., Roberts, M., Vidale, P. L., Vanniere, B., et al. (2021).  
632 Tropical cyclone precipitation in the HighResMIP atmosphere-only experiments of the  
633 PRIMAVERA Project. *Climate Dynamics*, 1, 3. [https://doi.org/10.1007/s00382-021-05707-](https://doi.org/10.1007/s00382-021-05707-x)  
634 x

635 Zhu, Y., Zhang, R. H., & Sun, J. (2020). North pacific upper-ocean cold temperature biases in  
636 CMIP6 simulations and the role of regional vertical mixing. *Journal of Climate*, 33(17),

637 7523–7538. <https://doi.org/10.1175/JCLI-D-19-0654.1>

638